Acta Crystallographica Section F
Structural Biology and Crystallization Communications
ISSN 1744-3091

Expression, purification and preliminary structural analysis of the coiled-coil domain of *Deinococcus radiodurans* RecN

Simone Pellegrino,[a] Daniele de Sanctis,[a] Sean McSweeney[a] and Joanna Timmins[b]*

[a]Structural Biology Group, European Synchrotron Radiation Facility, 6 Rue Jules Horowitz, F-38043 Grenoble, France, and [b]Virus Infection and Cancer Group/DNA Damage and Repair Team, Institut de Biologie Structurale J.-P. Ebel, 41 Rue Jules Horowitz, F-38027 Grenoble, France

Correspondence e-mail: joanna.timmins@ibs.fr

Received 18 October 2011
Accepted 22 December 2011

Deinococcus radiodurans has developed an efficient mechanism which allows the integrity of its entire genome to be fully restored after exposure to very high doses of ionizing radiation. Homologous recombination plays a crucial role in this process. RecN is a protein that belongs to the SMC-like protein family and is suggested to be involved in DNA repair. RecN is composed of a globular domain and an antiparallel coiled-coil region which connects the N- and C-termini. It has been suggested that dimerization of RecN occurs *via* the coiled-coil domain, but to date there is no structural or biochemical evidence for this. Here, SAXS studies and preliminary X-ray diffraction data of crystals of the purified coiled-coil domain of RecN are presented. The structure was solved by single-wavelength anomalous dispersion using SeMet derivatives, and preliminary electron-density maps support the rod-like model derived from the SAXS data. Model building and refinement are still ongoing.

1. Introduction

Deinococcus radiodurans has been classified as one of the most resistant organisms on earth. It tolerates high doses of ionizing radiation and withstands hundreds of double-strand breaks (DSBs), while in other organisms (such as *Escherichia coli*, *Saccharomyces cerevisiae*, humans *etc.*) just one or two DSBs are lethal. It is still unclear how this bacterium has developed such a strong tolerance. It might have evolved as a secondary effect of adaptation to desiccation (Cox & Battista, 2005).

RecA-mediated homologous recombination (HR) is the principal mechanism by which DSBs are accurately repaired. In *D. radiodurans* HR is achieved through the RecFOR pathway, since homologues of RecBC, which accomplish DNA recombination in *E. coli* (together with RecD), are missing (Singleton *et al.*, 2004).

RecN is also involved in recombinational repair and has been proposed to recognize DSBs (Sanchez *et al.*, 2006). RecN has been suggested to adopt a structural organization similar to the structural maintenance of chromosomes (SMC) proteins: a predicted ATP-binding cassette (ABC)-like globular head domain formed by the N- and C-terminal domains and a central coiled-coil region.

The overall structural organization is well conserved, but the length of the coiled-coil differs greatly between RecN and SMC proteins (Graumann & Knust, 2009). It is not yet understood whether the different lengths are related to the specific functions of these two protein families.

Dimer formation in SMC proteins is mediated through the coiled-coil domain and a recent study suggested that the coiled-coil region of RecN might be involved in dimerization or formation of even higher oligomeric states (Graumann & Knust, 2009). Dimerization is essential for regulation of dynamic DNA–protein interactions (Hirano & Hirano, 2002; Haering *et al.*, 2002).

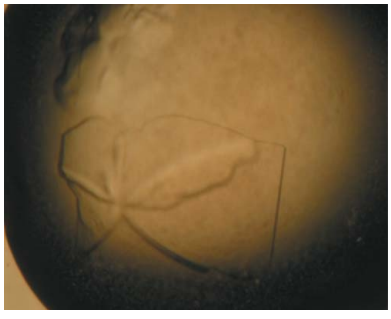

© 2012 International Union of Crystallography
All rights reserved

2. Materials and methods

2.1. DNA cloning and protein expression

DNA encoding the coiled-coil domain of *D. radiodurans* RecN was amplified from bacterial genomic DNA. A PCR reaction was carried

out using High Fidelity polymerase and the primers 5′-CACCCA-GCGCGAGCGGGCGCGG-3′ (forward) and 5′-TTACACATCGG-CTTGCAGGCTGCCCG-3′ (reverse). The PCR product was then cloned in a pET151-TOPO vector (Invitrogen), which contains a polyhistidine (6×) tag and a TEV cleavage site upstream of the gene-insertion region. Transformation of competent *E. coli* strain BL21* (DE3) cells (Invitrogen) was achieved by heat shock at 315 K. Cells containing the recombinant plasmid were grown in LB (lysogenic broth) medium supplemented with ampicillin at a final concentration of 0.1 g l^{-1}. The cultures were incubated at 310 K until the OD_{600} reached 0.6–0.8; 1 m*M* isopropyl *β*-D-1-thiogalactopyranoside (IPTG) was then added for induction of protein expression at 293 K overnight. The cells were subsequently harvested by centrifugation at 7548*g* for 30 min and resuspended in lysis buffer consisting of 50 m*M* Tris pH 8.0, 1 *M* NaCl, 5 m*M* $MgCl_2$, 5% glycerol.

2.2. Protein purification

Lysis was achieved by mechanical force in an SLM Aminco French pressure-cell press (10.13 MPa pressure limit). The lysate solution was centrifuged at 48 384*g* for 30 min and the resulting supernatant was collected and loaded onto a HisTrap HP column (GE Healthcare) equilibrated in buffer *A* (50 m*M* Tris pH 8.0, 300 m*M* NaCl, 5 m*M* $MgCl_2$, 5% glycerol, 5 m*M* imidazole). Extensive washing with buffer *A* (more than five column volumes) enabled the removal of the major contaminants from the column. The coiled-coil protein was eluted with a linear imidazole gradient of 0–100% buffer *B* (50 m*M* Tris pH 8.0, 300 m*M* NaCl, 5 m*M* $MgCl_2$, 5% glycerol, 500 m*M* imidazole) and eluted at about 115 m*M* imidazole. Fractions containing the coiled-coil protein were pooled and dialyzed overnight at 277 K against buffer *C* (50 m*M* Tris pH 8.0, 300 m*M* NaCl, 5 m*M* $MgCl_2$, 5% glycerol). At the same time, His-tag cleavage was achieved by the addition of TEV protease (to a final concentration of 0.1 mg ml^{-1}), 0.5 m*M* EDTA and 1 m*M* DTT. There was no obvious precipitation after dialysis and the protein was thus concentrated to 15 mg ml^{-1} using Amicon Ultra centrifugal concentrators (Millipore, 10 000 molecular-weight cutoff) and loaded onto a Superdex 200 column (GE Healthcare) equilibrated in buffer *C*. The gel-filtration step yielded a highly pure coiled-coil sample (Fig. 1). Prior to structural studies, the polydispersity of the sample was determined by dynamic light scattering (DLS) using a Zetasizer Nano (Malvern Instruments Ltd, UK).

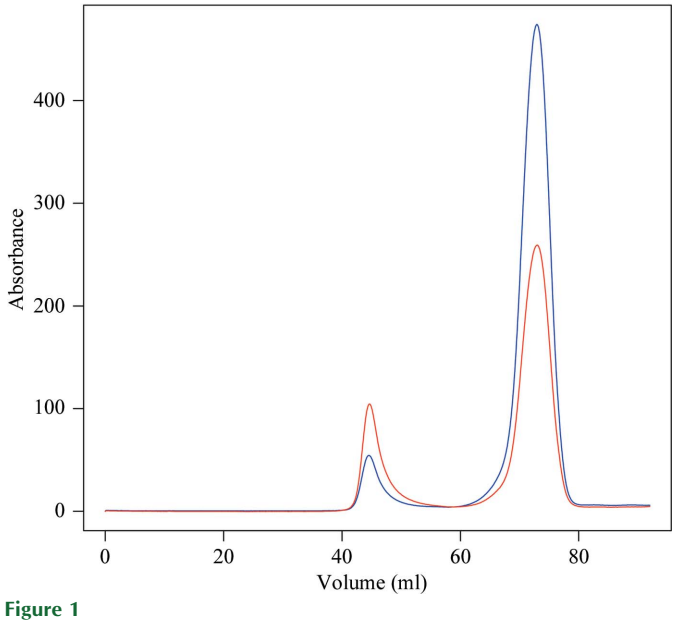

Figure 1
Size-exclusion chromatography profile of the coiled-coil domain of RecN. Absorbance at 280 nm (blue) and 260 nm (red) is shown. The single protein peak indicates that the coiled coil is homogeneous.

2.3. Small-angle X-ray scattering

Small-angle X-ray scattering (SAXS) experiments were performed on the ID14-3 beamline (Pernot *et al.*, 2010) at the European Synchrotron Radiation Facility (ESRF), Grenoble using a fixed energy of 13.32 keV (λ = 0.931 Å) and employing a Pilatus 1M pixel detector (Dectris, Switzerland). Measurements were performed at three different protein concentrations (5.99, 2.95 and 1.48 mg ml^{-1})

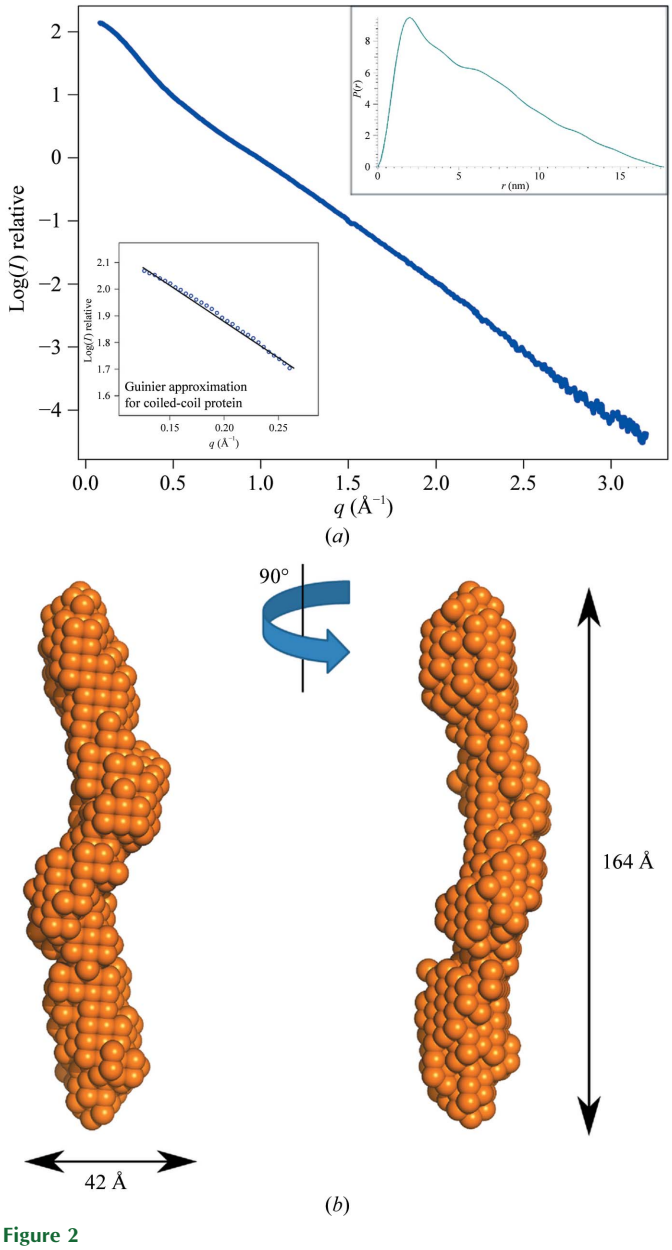

Figure 2
(*a*) Experimental scattering curve of the coiled-coil domain of RecN and its relative pair distribution function *P*(*r*) (*I*, intensity; *S*, momentum transfer; *r*, d_{max}). The scattering curve was derived by merging the highest concentration curve with the lowest concentration curve. (*b*) The averaged model obtained for the coiled-coil domain is shown in two orientations 90° apart. The length and width of the envelope are indicated.

to verify that no interparticle effects are observed that could invalidate the analysis. Protein concentration was calculated using the extinction coefficient and by reading the absorption at 280 nm in a Nanodrop 1000 spectrophotometer (Thermo Scientific, USA).

In order to exclude radiation damage, ten frames of 10 s duration each were collected while continuously exposing fresh sample to the X-ray beam. The resulting frames were then overlaid in order to detect any differences arising from exposure to X-ray photons. Data for the buffer solution were also collected and processed for subtraction from the scattering curves of the samples. All data were integrated and processed using tools in the *ATSAS* software package (Petoukhov *et al.*, 2007). *Primus* (Konarev *et al.*, 2003) was used to estimate the radius of gyration (R_g) after detection of the data range which fits the Guinier approximation (Fig. 2). The distance distribution function $P(r)$ was computed using *GNOM* (Svergun, 1992). Experimental data were used for *ab initio* model building using *GASBOR* (Svergun *et al.*, 2001) to determine the protein solution envelope (Fig. 2), applying a twofold axis as a symmetry restraint. The *DAMAVER* package (Volkov & Svergun, 2003) was then used to align the 22 independent *ab initio* models generated, to average them and to filter the averaged model at a given cutoff volume.

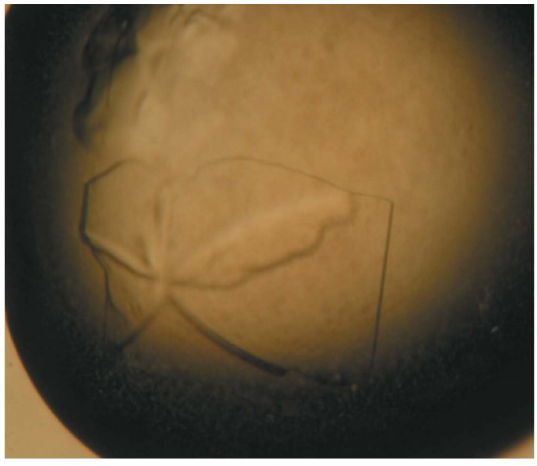

(*a*)

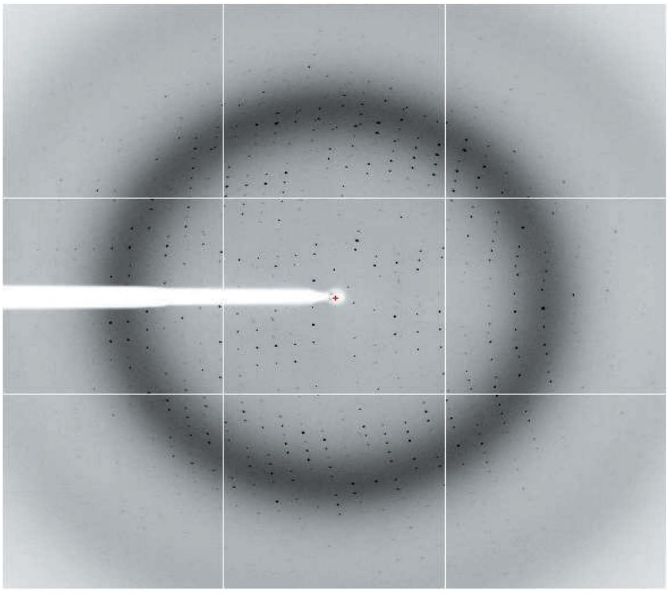

(*b*)

Figure 3
(*a*) RecN coiled-coil domain crystals. Plates were obtained after 2 d equilibration of the drop against the precipitant solution. (*b*) Typical diffraction pattern of native coiled-coil crystals collected on ID23-1 at the ESRF.

Table 1
Data-collection statistics.

Values in parentheses are for the highest resolution shell.

	Native	Se peak
Beamline	ID23-1, ESRF	ID14-4, ESRF
Space group	$P2_1$	$P2_1$
Unit-cell parameters (Å, °)	a = 73.21, b = 43.97, c = 133.63, $\alpha = \gamma$ = 90.00, β = 97.71	a = 71.57, b = 45.44, c = 133.42, $\alpha = \gamma$ = 90.00, β = 97.47
Resolution range (Å)	52.5–2.04 (2.15–2.04)	66.2–2.28 (2.40–2.28)
Oscillation range (°)	1.0	1.0
Wavelength (Å)	0.992	0.9795
Mosaicity (°)	0.73	0.48
Total No. of reflections	125244 (17409)	174025 (25304)
No. of unique reflections	52532 (7683)	39476 (5691)
Completeness (%)	97.1 (98.2)	99.6 (99.7)
R_{merge}† (%)	7.0 (32.1)	7.4 (22.8)
$R_{r.i.m.}$‡ (%)	8.8 (41.3)	10.2 (30.1)
$R_{p.i.m.}$§ (%)	5.3 (25.6)	4.8 (14.1)
Mean $I/\sigma(I)$	8.4 (2.8)	12.4 (5.2)
Multiplicity	2.4 (2.4)	4.4 (4.4)
Anomalous multiplicity		2.3 (2.3)
Molecules per asymmetric unit	4	4
V_M (Å^3 Da^{-1})	2.96	2.83
CC_{anom}¶		39.1
SHELXD (CC_{all}/CC_{weak})		34.00/26.11
FOM (substructure)†† (%)		42
FOM (phasing)‡‡ (%)		65

† $R_{merge} = \sum_{hkl}\sum_i |I_i(hkl) - \langle I(hkl)\rangle| / \sum_{hkl}\sum_i I_i(hkl)$, where $I(hkl)$ is the integrated intensity for a given reflection. ‡ $R_{p.i.m.} = \sum_{hkl}\{1/[N(hkl)-1]\}^{1/2}\sum_i |I_i(hkl) - \langle I(hkl)\rangle| / \sum_{hkl}\sum_i I_i(hkl)$. § $R_{r.i.m.} = \sum_{hkl}\{N(hkl)/[N(hkl)-1]\}^{1/2}\sum_i |I_i(hkl) - \langle I(hkl)\rangle| / \sum_{hkl}\sum_i I_i(hkl)$. ¶ Correlation coefficient from *SHELXC*. †† Figure of merit from *SHELXD*. ‡‡ Figure of merit from *RESOLVE*.

2.4. Crystallization

The RecN coiled-coil domain was used for initial crystallization screening at concentrations of 7.7 and 14.82 mg ml^{-1} at 293 K in Greiner CrystalQuick sitting-drop vapour-diffusion plates. A Cartesian PixSys 4200 crystallization robot (Genomic Solutions, UK) facility (High Throughput Crystallization Laboratory at EMBL Grenoble) was used to dispense 200 nl drops consisting of equal volumes of protein and reservoir solutions as described in Dimasi *et al.* (2007). The following commercial screens were set up: Crystal Screen, Crystal Screen 2, Crystal Screen Lite, PEG/Ion, MembFac, Natrix, QuickScreen, Grid Screens (Ammonium Sulfate, Sodium Malonate, Sodium Formate, PEG 6K, PEG/LiCl, MPD) and Index (Hampton Research, Aliso Viejo, California, USA). Initial crystals appeared in condition No. 15 of Grid Screen PEG/LiCl. Scale-up of the crystallization trial was performed manually and crystals of higher quality were obtained after further optimization of the pH (6.5–9) and the PEG 6K concentration (15–30%) and finally by the use of Additive Screen (Hampton Research) (Fig. 3).

Crystals that diffracted to 2.04 Å resolution were obtained from droplets in which 1 µl protein solution (at 13.5 mg ml^{-1}) was mixed with 1 µl reservoir solution consisting of 0.1 *M* HEPES pH 7, 30% PEG 6000, 1 *M* LiCl, 3% 1,2,3-heptanetriol.

2.5. X-ray diffraction analysis and structure determination

X-ray diffraction experiments were performed on suitable crystals on the ID14-4 (McCarthy *et al.*, 2009) and ID23-1 (Nurizzo *et al.*, 2006) beamlines at the ESRF, Grenoble. Glycerol was added at a concentration of 25% to the mother liquor as a cryoprotectant. Diffraction data were collected at 100 K using an X-ray wavelength of 0.9795 Å and an ADSC Q315R detector.

Since the coiled-coil region shows only very low sequence similarity to other known structures, SeMet-derivatized protein was overexpressed (Doublié, 1997) and purified following the protocol described in §2.2. Crystals were obtained under the same conditions as used for the native protein.

A complete data set was collected at the selenium absorption peak (12.658 keV) in order to perform a single-wavelength anomalous dispersion (SAD) experiment. Integration of the diffraction spots and processing were performed using *iMOSFLM* (Battye *et al.*, 2011). Averaged intensities for each reflection were obtained with *SCALA* (Evans, 2006), while estimation of amplitudes $|F|$ from intensities I was achieved with *CTRUNCATE* (French & Wilson, 1978) (Table 1).

Determination of the Matthews coefficient (Matthews, 1968) was carried out using the *MATTHEWS_COEF* program (Kantardjieff & Rupp, 2003), resulting in a solvent content of 56.5% corresponding to four molecules in the asymmetric unit. The structure-factor file was then submitted to *Auto-Rickshaw* (Panjikar *et al.*, 2005), which used the programs listed below to solve the protein structure.

Positioning of heavy-atom sites and initial phasing was performed using the *SHELX* package (Sheldrick, 2010). *SHELXD* successfully placed all four predicted selenium sites, resulting in a clear solution (CC_{all} = 34.00/CC_{weak} = 26.11). *SHELXE* identified the correct substructure hand and calculated initial phases and density improvement (FOM of 0.676). Autotracing implemented in *SHELXE* started to build polyalanine chains in the electron-density map, but the resulting model was incomplete. *DM* (Cowtan, 2010) and *RESOLVE* (Terwilliger, 2000) were run for further density modification of the experimental electron-density map. Partial model building was carried out by *ARP*/*wARP* (Langer *et al.*, 2008), which docked 523 of the 592 (86% of the total number) residues built after 14 cycles.

3. Results and discussion

The RecN coiled-coil domain was purified to homogeneity. Quality control of the sample prior to structural studies was achieved using SEC and DLS. The theoretical molecular weight of the coiled-coil domain is 18 kDa. An SEC calibration curve was used to estimate the molecular weight of the protein based on its elution volume. The coiled-coil domain eluted at 72.8 ml, corresponding to a molecular weight of approximately 65 kDa and indicating that the coiled-coil domain is oligomeric (Fig. 1). This high value can most likely be explained by the elongated shape of the coiled-coil domain of RecN, which would be more retarded on the SEC matrix compared with a globular protein of the same molecular weight. DLS measurements revealed that the purified coiled-coil domain is monodisperse (PdI < 0.2), with an estimated hydrodynamic radius of 4.33 nm.

The RecN coiled-coil domain was used for SAXS studies (Fig. 2). The radius of gyration was calculated to be 4.73 nm and its estimated molecular weight, after comparison with the I_0 (scattering intensity at zero angle) of BSA, was found to be ∼37 kDa, which corresponds to a dimeric assembly and is consistent with the data measured by DLS. The difference between the two experimental results may arise from the different methods of calculation (Putnam *et al.*, 2007) and the shape of the molecule. *Ab initio* modelling using *GASBOR* resulted in an elongated model (Fig. 2), which is in agreement with previous data reported in the literature (Melby *et al.*, 1998; van Noort *et al.*, 2003) and suggests that the coiled-coil domains of SMC proteins adopt rod-like structures.

The native coiled-coil domain of RecN was successfully crystallized (Fig. 3). The crystals diffracted to 2.04 Å resolution and belonged to space group $P2_1$, with unit-cell parameters a = 73.21, b = 43.97, c = 133.63 Å, β = 97.71° (Table 1). After unsuccessful attempts to solve the structure by molecular replacement, selenomethionine-derivatized protein was overexpressed, purified and crystallized. The crystals were cryoprotected in precipitant solution supplemented with 25% glycerol and then directly mounted on a mini-diffractometer. The crystals diffracted to 2.28 Å resolution and a complete anomalous data set was therefore collected at the selenium absorption peak in order to maximize the anomalous signal in the data. The structure was solved using the SAD method and automated building yielded a 75% complete model. The electron-density map after density modification was easily interpretable and is reminiscent of the rod-like structure derived from our SAXS data (Fig. 2). Final rounds of manual building and refinement against native data (collected at 2.04 Å resolution) are in progress.

The data for this work were collected at the ESRF on the ID14-3 beamline for the SAXS analysis and on the ID14-4 and ID23-1 beamlines for the crystallographic part. We thank the beamline staff for assistance and advice during data collection.

References

Battye, T. G. G., Kontogiannis, L., Johnson, O., Powell, H. R. & Leslie, A. G. W. (2011). *Acta Cryst.* D**67**, 271–281.
Cowtan, K. (2010). *Acta Cryst.* D**66**, 470–478.
Cox, M. M. & Battista, J. R. (2005). *Nature Rev. Microbiol.* **3**, 882–892.
Dimasi, N., Flot, D., Dupeux, F. & Márquez, J. A. (2007). *Acta Cryst.* F**63**, 204–208.
Doublié, S. (1997). *Methods Enzymol.* **276**, 523–530.
Evans, P. (2006). *Acta Cryst.* D**62**, 72–82.
French, S. & Wilson, K. (1978). *Acta Cryst.* A**34**, 517–525.
Graumann, P. L. & Knust, T. (2009). *Chromosome Res.* **17**, 265–275.
Haering, C. H., Löwe, J., Hochwagen, A. & Nasmyth, K. (2002). *Mol. Cell*, **9**, 773–788.
Hirano, M. & Hirano, T. (2002). *EMBO J.* **21**, 5733–5744.
Kantardjieff, K. A. & Rupp, B. (2003). *Protein Sci.* **12**, 1865–1871.
Konarev, P. V., Volkov, V. V., Sokolova, A. V., Koch, M. H. J. & Svergun, D. I. (2003). *J. Appl. Cryst.* **36**, 1277–1282.
Langer, G., Cohen, S. X., Lamzin, V. S. & Perrakis, A. (2008). *Nature Protoc.* **3**, 1171–1179.
Matthews, B. W. (1968). *J. Mol. Biol.* **33**, 491–497.
McCarthy, A. A., Brockhauser, S., Nurizzo, D., Theveneau, P., Mairs, T., Spruce, D., Guijarro, M., Lesourd, M., Ravelli, R. B. G. & McSweeney, S. (2009). *J. Synchrotron Rad.* **16**, 803–812.
Melby, T. E., Ciampaglio, C. N., Briscoe, G. & Erickson, H. P. (1998). *J. Cell Biol.* **142**, 1595–1604.
Noort, J. van, van der Heijden, T., de Jager, M., Wyman, C., Kanaar, R. & Dekker, C. (2003). *Proc. Natl Acad. Sci. USA*, **100**, 7581–7586.
Nurizzo, D., Mairs, T., Guijarro, M., Rey, V., Meyer, J., Fajardo, P., Chavanne, J., Biasci, J.-C., McSweeney, S. & Mitchell, E. (2006). *J. Synchrotron Rad.* **13**, 227–238.
Panjikar, S., Parthasarathy, V., Lamzin, V. S., Weiss, M. S. & Tucker, P. A. (2005). *Acta Cryst.* D**61**, 449–457.
Pernot, P., Theveneau, P., Giraud, T., Fernandes, R. N., Nurizzo, D., Spruce, D., Surr, J., McSweeney, S., Round, A., Felisaz, F., Foedinger, L., Gobbo, A., Huet, J., Villard, C. & Cipriani, F. (2010). *J. Phys. Conf. Ser.* **247**, 012009.
Petoukhov, M. V., Konarev, P. V., Kikhney, A. G. & Svergun, D. I. (2007). *J. Appl. Cryst.* **40**, s223–s228.
Putnam, C. D., Hammel, M., Hura, G. L. & Tainer, J. A. (2007). *Q. Rev. Biophys.* **40**, 191–285.
Sanchez, H., Kidane, D., Castillo Cozar, M., Graumann, P. L. & Alonso, J. C. (2006). *J. Bacteriol.* **188**, 353–360.
Sheldrick, G. M. (2010). *Acta Cryst.* D**66**, 479–485.
Singleton, M. R., Dillingham, M. S., Gaudier, M., Kowalczykowski, S. C. & Wigley, D. B. (2004). *Nature (London)*, **432**, 187–193.
Svergun, D. I. (1992). *J. Appl. Cryst.* **25**, 495–503.
Svergun, D. I., Petoukhov, M. V. & Koch, M. H. J. (2001). *Biophys. J.* **80**, 2946–2953.
Terwilliger, T. C. (2000). *Acta Cryst.* D**56**, 965–972.
Volkov, V. V. & Svergun, D. I. (2003). *J. Appl. Cryst.* **36**, 860–864.